Pion-Proton Scattering below 150 Mev. I*

S. W. Barnes, B. Rose,† G. Giacomelli,‡ J. Ring, K. Miyake, and K. Kinsey
University of Rochester, Rochester, New York

(Received July 16, 1959)

Positive-pion proton differential cross sections have been measured at 41.5 Mev for six angles. The angles in the center-of-mass system are 53°, 69.1°, 100.4°, 128°, 141.7°, and 163.5° and the corresponding cross sections in mb/sterad in the center-of-mass system are 0.252±0.020, 0.354±0.025, 0.777±0.038, 1.145 ±0.067, 1.495±0.084, and 1.750±0.110. Negative pion elastic cross sections have been measured for the first five of the above angles and are, respectively, in mb/sterad in the c.m. system: 0.338±0.047, 0.281 ±0.038, 0.148±0.029, 0.112±0.042, and 0.085±0.25. Phase-shift analyses of these data and those of other authors lead to the following expressions for the low-energy behavior of the $T=\frac{3}{2}$ phases: $\alpha_{31}{}^{N}=-(0.0418 \pm 0.004)\eta^3$, $\alpha_3{}^{N}=-(0.1145\pm 0.0026)\eta$, and $\cot\alpha_{33}{}^{N}=\frac{4}{3}\eta^3\,(0.0877\pm 0.0014)/[\omega^*(1-\omega^*/2.17)]$.

I. INTRODUCTION

THE pion-proton interaction, being fundamental to an understanding of classical nuclear physics, has been vigorously investigated since the first pion beams became available for experiments. In these, differential and total cross-section measurements have been made at ever increasing energies and with increasing accuracy. Early analyses employing S and P waves and assuming charge independence led to various sets of phase shifts. Later studies selected the Fermi-type set with its positive and dominant α_{33} which accounted for the first resonance observed in positive pion scattering. The signs and the energy dependencies of the other major phases were set but the minor ones were less well specified. The work reported here is limited to a study of the behavior of the phases at energies below the $T=J=\frac{3}{2}$ resonance. Analyses reported below of recent data of this laboratory[1–4] and other laboratories[5–7] taken at energies up to 150 Mev show agreement with the energy dependencies generally assumed for the $T=\frac{3}{2}$ phases but show some differences from those for the $T=\frac{1}{2}$ phases and appear to define even the minor phase shifts within this energy region.

Part I of this paper is devoted to the measurements of positive and negative pion-proton differential cross sections which were made at a mean energy of 41.5 Mev. This is followed by a discussion of the phase-shift analysis used and then analyses of various combinations of data are given. These lead (*a*) to the conclusion that no fault can be found with the momentum dependencies usually assumed for the $T=\frac{3}{2}$ phases and (*b*) to a fairly precise determination of α_{31}.

In Part II we describe the two differential measurements that were made to complete a π^- distribution at 30 Mev and proceed to the analysis of the π^- distributions which are available at 30, 41.5, 98, and 150 Mev. These individual analyses indicate certain empirical momentum dependencies for the $T=\frac{1}{2}$ phases in the energy region from 20 to 150 Mev but are not considered to have any validity for higher energies. Various quantities are then calculated and compared with published experimental values.

II. EXPERIMENTAL ARRANGEMENT

The pions for the 41.5-Mev scattering experiments emerged from a thin window in the cyclotron tank and traveled a helium path through a 3-ft brass shield on into a magnetic deflecting and focusing field, and from there through further lead shielding to the approximate focus, where they emerged into air and were counted by a conventional incident telescope of two small disk-shaped Scintillon counters (see Fig. 1). The available currents amounted to 1 to 2.5×10^4 pions per minute. Since the current of scattered pions depends upon the incident current, the cross section, the number of

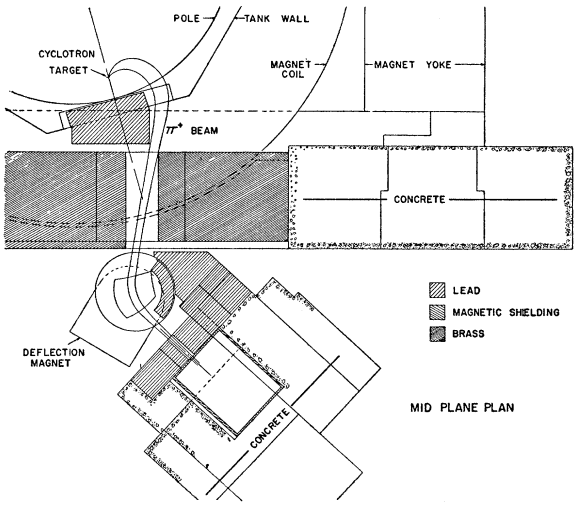

FIG. 1. Layout of cyclotron and shielding for 41.5-Mev meson beam.

* Supported in part by the U. S. Atomic Energy Commission.
† On leave from and now returned to Atomic Energy Research Establishment, Harwell, Berkshire, England.
‡ Now at Istituto Di Fisica "A. Righi," Della Universita Degli Studi Di Bologna, Bologna, Italy.
[1] W. J. Spry, Phys. Rev. **95**, 1295 (1954).
[2] W. B. Johnson and M. Camac (to be published).
[3] J. Ring and D. Miller (to be published).
[4] G. Giacomelli (to be published).
[5] Bodansky, Sachs, and Steinberger, Phys. Rev. **93**, 1367 (1954).
[6] Ashkin, Blaser, Feiner, and Stern, Phys. Rev. **101**, 1149 (1956).
[7] S. L. Leonard and D. H. Stork, Phys. Rev. **93**, 568 (1954).

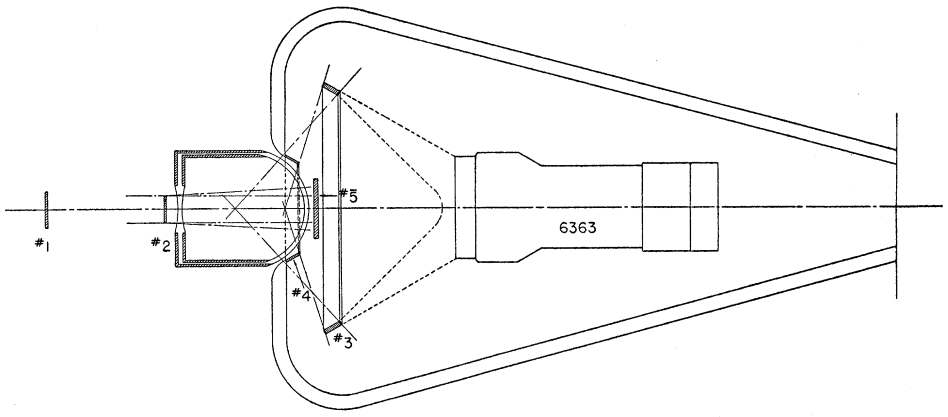

FIG. 2. 45° scattering layout.

target protons/cm², and the solid angle of the scattering telescope, and each of the first three quantities was small, it was necessary to make the last large. This was done by building a special scattering telescope of large solid angle for each angle of scattering. The mean angles in the laboratory system were 45°, 60°, 90°, 120°, 135° and 160°. The detecting telescope for pions scattered at 45° and 60° consisted of pairs of annular crystals; those used for the other angles had somewhat less than 2π annularity. The upper limit to the solid angle in each case (except that of 160°) was set by the requirement that the angular spread $d\theta$ of the pions accepted by the scattering telescope should be small enough to exclude pions scattered from the walls of the hydrogen target. Since further gains in solid angle accrued from the use of different shapes of targets for particular angles of scattering, 3 liquid hydrogen targets were used and are referred to here as the cylindrical, "spherical," and "plane" targets.

Figure 2 indicates the arrangement used in the 45° measurements where all the pions scattered from a central point in the "spherical" hydrogen target in the angular range from 37° to 53° were detected without the inclusion of any pions from the target walls. This spherical target was also used for scattering at 60° and 135°; see Figs. 3 and 4. It was replaced in the 90° scattering arrangement by a cylindrical target shown in Fig. 5. Figure 6 gives the 90° scattering arrangement. The cylindrical target was again used in the 120° scattering runs, the geometry being indicated in Fig. 7. Finally a "plane" target was constructed for the 160° measurement, the arrangement of crystals, beam, and target being shown in Fig. 8. In this case the detecting telescope received pions scattered by the target walls as well as by the hydrogen.

Figure 9 is a simplified block diagram of the electronics. A signal from a photomultipler passes first through an adjustable delay and attenuator and then is amplified. Further amplification is provided by a Clark amplifier (not shown) just before the trigger generators. The trigger circuits use secondary emission EFP-60 tubes and produce a standard output pulse of 30 mμsec in width. The trigger generator marked with a star produces a pulse of about 75 mμsec duration. The coincidence circuits are of the Rossi type and have an effective resolving time (2τ) of about 45 mμsec (about 100 mμsec for the anticoincidence—denoted by a bar over the number). These numbers refer to the full width of the delay curves. The output from the $1234\bar{5}$ coincidence causes the gated amplifier to operate, feeding the signal from counters No. 3 into the 24-channel analyzer.

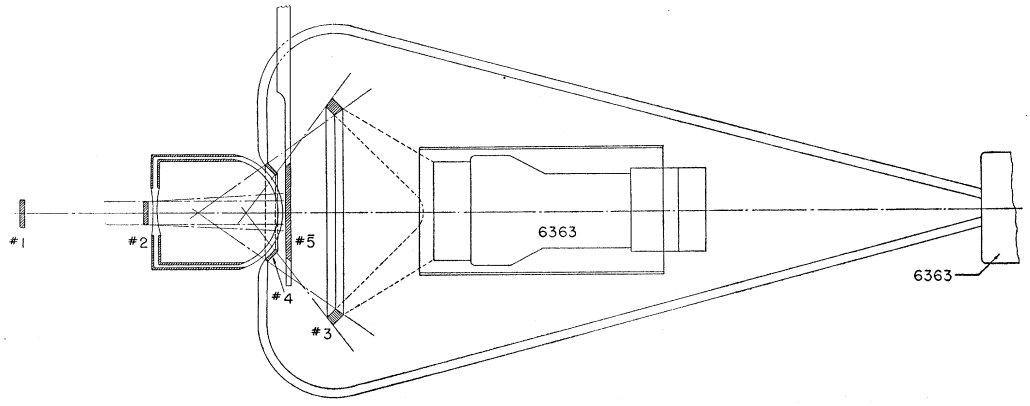

FIG. 3. 60° scattering layout.

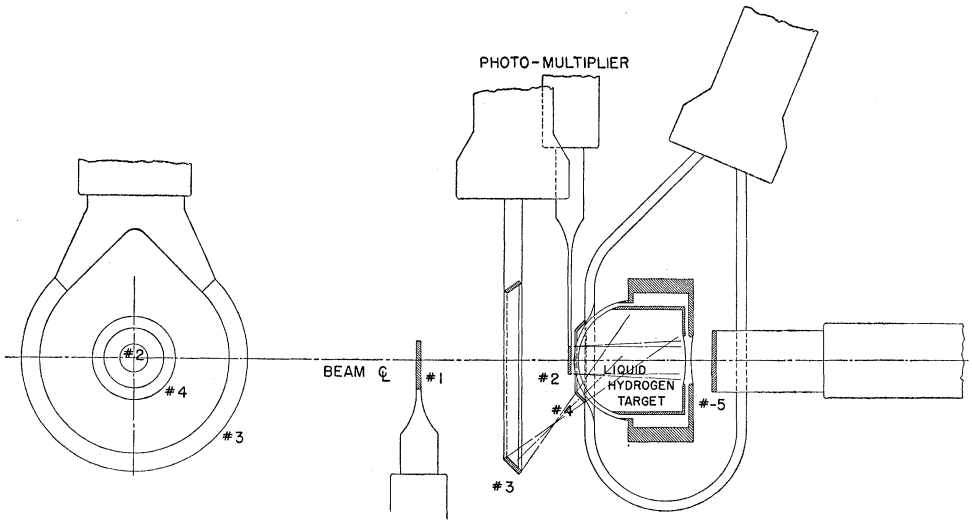

FIG. 4. 135° scattering layout.

Counts corresponding to a (1234) coincidence, 5 anti-coincidence are called "fulls" if obtained when liquid hydrogen filled the scattering chamber—"empties" if the chamber contained either hydrogen vapor or a mixture of He gas and hydrogen vapor at atmospheric pressure. The number of hydrogen scattering events in any run is assumed to be closely related to the difference between the Full and Empty counts. Since the validity of this assumption must improve as the Empty counts diminish with respect to the Fulls, efforts were made to keep the former small.

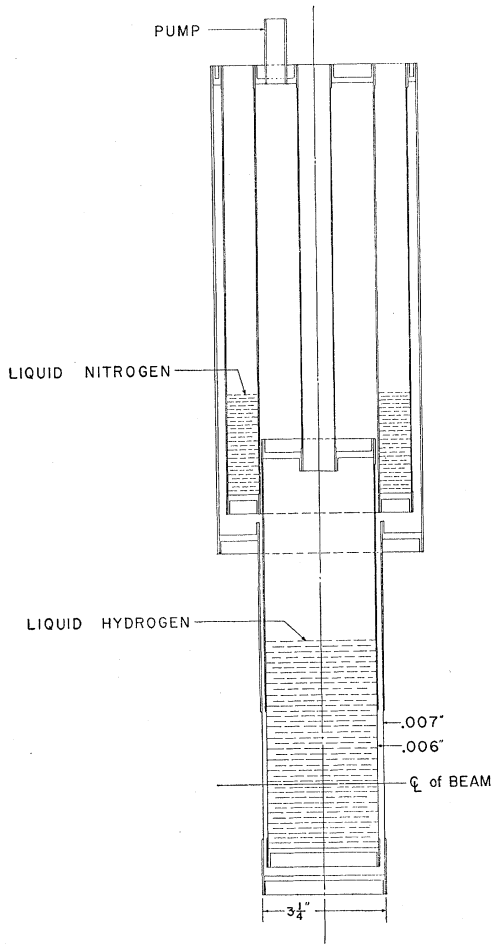

FIG. 5. Cylindrical liquid hydrogen target.

The "no wall scattering" feature together with the extensive shielding used reduced the empty counts to a few percent of the full counts for π^+ scattering. The full to empty counting ratio was further improved by making a pulse-height analysis of the counts from one of the two crystals in the scattering telescope. The scattered pion pulses formed a peak which was contained in roughly half the channels, while the empty pulses were distributed more or less evenly through all channels so that the full and empty ratio was approximately twice what it would have been without the pulse-height analysis. Figure 10 displays the pulse-height distributions observed in a typical 60° scattering run. These curves are representative; at some angles the pulse-height resolution was better, at some it was slightly poorer. When the pion-hydrogen cross section was least, that is in the π^- backward scattering, the empty counts at times amounted to a third or even a half of the full counts. In taking the difficult backward π^- points, the run was begun with positive pions to establish the shape and position of the pion pulse-height distribution, then the magnetic fields were reversed to give negative pions and the scattering of the negative pions first from the full, then the empty target was recorded for several alternations, after which the run was interrupted for a check with positive pions.

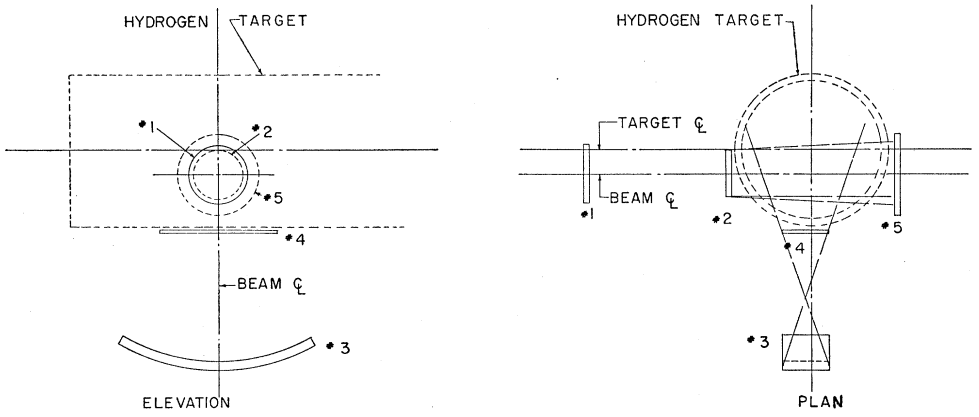

FIG. 6. 90° scattering layout.

III. ENERGY AND CONTAMINATION OF THE PION BEAMS

The energy of the pion beam was determined in the usual manner from a range curve. The effective contamination of the beam by muons and electrons depended upon the gains of the two counters of the incident telescope. The electron contamination was determined as follows: the gains of counters No. 1 and No. 2 were set at a high value and a range curve taken. The tail of this curve showed a large and accurately measurable number of electrons. A pulse-height distribution of the pulses of one of the counters in the incident telescope was then taken. This distribution consisted of two peaks satisfactorily separated, the lower being due to electrons, the upper to muons and pions, and so gave the fraction of doubles counts in the incident beam which were due to electrons. This fraction was compared to the number found in the tail of the range curve and the ratio recorded. The gains of No. 1 and No. 2 were then lowered until the tail of a range curve showed only a small number of electrons and the above ratio was applied to give the fraction in the incident beam. The gains of No. 1 and No. 2 were carefully held at this last setting during the run, and occasional interruptions were made to check that the contamination had not changed. The muon contamination of $3\pm2\%$ was directly apparent from the range curve taken with No. 1 and No. 2 running at their operating gains.

IV. EVALUATION OF CROSS SECTIONS

The number of scattering events per second is given by

$$N=\sigma\epsilon\int_V n_p n_\pi \Omega dV,$$

where n_p is the number of hydrogen nuclei per cm^3, n_π is the incident pion flux in particles cm^{-2} sec^{-1}, Ω is the solid angle subtended by the detecting telescope at the point concerned, σ is the differential cross section in cm^2 sterad^{-1}, ϵ is the efficiency of detection of the scattered pions and the integral is taken over the volume of the liquid hydrogen target.

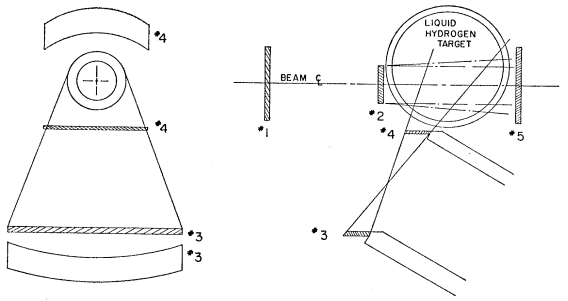

FIG. 7. 120° scattering layout.

The region of the target that contributes to the integral is defined by the beam diameter and by the

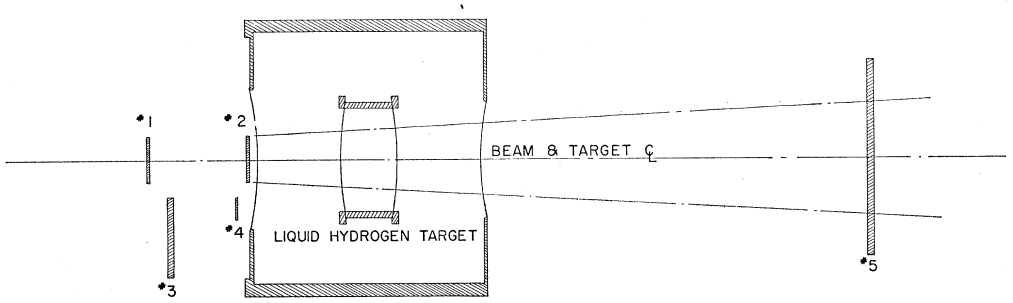

FIG. 8. 160° scattering layout.

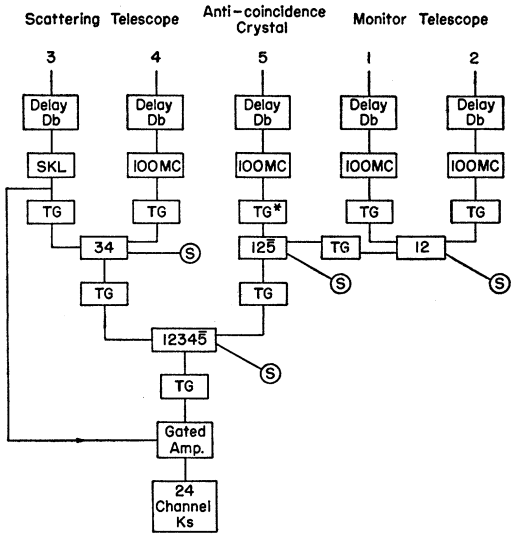

FIG. 9. Simplified block diagram of the electronics.

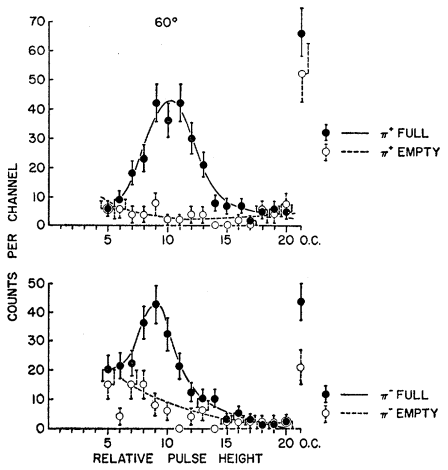

FIG. 10. Pulse-height distribution of mesons scattered at 60° during a typical run.

detecting crystals 3 and 4 only, except in the case of scattering at 160° where the beam diameter, crystal 3, and the ends of the target define the contributing region. In each case the integral may be used to define a quantity S given by:

$$SN_\pi n_p = \int_V n_p n_\pi \Omega dV,$$

where N_π is the total number of incident pions per second. If we now define ν as the number of scattering events per million incident mesons, which is a convenient experimental quantity, it may readily be shown that, for a liquid hydrogen density of 0.071 g cm^{-3},

$$\sigma = 2.357 \times 10^{-2}(\nu/\epsilon S) \text{ mb sterad}^{-1}.$$

S was evaluated for each scattering angle by both graphical and numerical methods. The agreement between the two methods was better than 2%, and the mean value of the two was taken. The value of S was calculated on the assumption that the solid angle was determined by the mid-planes (or the mid-surfaces) of the relevant detecting crystals 3 and 4.

A meson passing through the mid-plane, even if it emerged through an edge rather than through the front or back faces, would give a pulse whose height was greater than half of that of a meson which passed normally through the crystal from front to back (*a* "normal" pulse). Ideally only those pulses should be accepted which were greater than half the "normal" pulse. In practice the bias on channel No. 4 was not set at this point, but a small correction was applied based on a calculation of the edge effect in that crystal. This correction never exceeded 2%. The bias in channel 3, the pulse-height channel, was always a set at about a quarter of the "normal" pulse height, but only pulses greater than half, and less than one and a half, times the "normal" pulse height were included in the totals.

A correction was also necessary for the high pulse-height cutoff. This correction was calculated from the theory of Symon[8] to be about 1½%. Support for this figure was also found from analysis of our π^+ data, which showed that the pulses due to hydrogen which exceeded the high pulse-height cutoff were (2.0±1.0)% of the total counts due to hydrogen, of which an estimated 0.8% would be due to stars. The corresponding figure for the π^- data was (0.6±2.9)% when corrected for stars. Consequently a correction of (1.5±1)% was added for this effect.

The π^- cross sections at 90°, 120°, and 135° were evaluated in terms of their ratios to the π^+ cross sections at the same energy, by comparison of the number of counts in corresponding pulse-height analyzer channels. The reason for doing this was that, in general, the background counts in the low channels were relatively much greater in the π^- runs. Consequently, by eliminating the low channels from the data, the background was much reduced and the statistical accuracy improved. The channels included in the analysis are indicated in Fig. 10.[9]

[8] K. R. Symon, in B. Rossi, *High-Energy Particles* (Prentice Hall, Inc., New York, 1952), Sec. 2.7, p. 32; K. R. Symon, thesis, Harvard University, 1948 (unpublished).

[9] We have assumed that the background counts were unaffected by the presence or absence of hydrogen in the target. This was based on the following facts: (a) The overcount, that is the number of counts greater than one and a half times the most probable pulse height, was the same with target full or empty, apart from the expected small contribution from the high-energy tail of the pulse-height distribution. (b) The number of "full" minus "empty" counts between the low-energy cutoff and the hydrogen peak could be quantitatively explained in terms of the expected edge effect in the pulse-height crystal. (For π^- mesons there would be an additional contribution from electrons in this range.) (c) Calculation of the background indicated that probably the greatest contribution would arise from two-pronged stars in crystal 2, the two prongs passing through crystals No. 3 and No. 4, respectively. This was qualitatively borne out by examination of the background to the 135° π^+ run in which there is a bump beginning directly below the hydrogen peak. This bump, and the accompany-

TABLE I. Geometrical factors and data from typical runs.[a]

θ	$\Delta\theta$	S (steradians, c.m. system)	$\nu(\pi^+)$ Full	$\nu(\pi^+)$ Empty	$\nu(\pi^-)$ Full	$\nu(\pi^-)$ Empty	Number of runs π^+	Number of runs π^-
53.0	20°	0.878	13.5±1.2	2.4±0.8	21.4±2.0	5.3±1.6	2	2
69.1	27°	1.626	35.5±2.1	5.7±1.2	40.2±3.5	19.5±2.5	1	1
100.4	29°	0.935	27.0±2.1	0	5.1±0.8	0.4±0.3	4	2
128.0	21°	0.294	12.4±0.8	0.9±0.4	2.0±0.6	0.5±0.4	2	2
141.7	18°	0.974	52.6±1.9	9.2±1.2	4.3±0.8	2.0±0.6	1	1
163.5	30°	0.421	31.6±1.6	9.3±1.2			3	...

[a] θ is the mean c.m. scattering angle. $\Delta\theta$ is the base width of the angular resolution function, which is approximately triangular for all angles. S is the effective target length multiplied by the solid angle subtended at the target by the scattering telescope and is defined precisely in Sec. IV. ν is the number of counts registered in the appropriate pulse-height interval per million mesons incident on the beam telescope, for typical runs.

Small corrections were applied for counting losses and for the fact that the target during an "empty" run was full of hydrogen vapor at 20°K, which has a density of 1.7% of that of liquid hydrogen. Corrections varying from 2% to 4% were applied for absorption of the beam in the target walls, the liquid hydrogen, and the crystals 3 and 4.

No correction was applied for the decay of the beam after scattering because (a) roughly as many muons decay "into" the scattering telescope as decay "out" of it and the pulse-height resolution was such that these muons would in general be indistinguishable from the scattered pions and (b) the total decay after scattering was less than 2%. Consequently any error introduced is extremely small.

A further correction arose from the fact that the observed distribution of mesons across the beam (the "traverse" curve) was in general different from the ideal distribution assumed in the calculation of the quantity S. This was in general less than 1%, and was only larger than this in the case of scattering at 90° where the crystal geometry did not have cylindrical symmetry about the meson beam.

In the case of π^- data, corrections were necessary because of the probability of detection of electron pairs following exchange scattering. For scattering into the forward angles, the energy loss of a high-energy electron pair is approximately the same as that of the scattered mesons so that our pulse-height selection did not help to discriminate against electron pairs. At backward angles, however, the meson energy loss is considerably enhanced and appreciable discrimination was achieved. The correction was calculated on the basis of the known exchange scattering cross section for π^- mesons at 40 Mev, and on the probability of production of electron pairs either in the π^0-decay process or by conversion in the material of the target. The correction was always less than 0.04 mb. An attempt was made at 120° scattering angle to make a direct determination of the effect of counting electron pairs, by introducing lead at the target wall to increase the total production of electron pairs by a factor of seven, and in the limited time available for this test the counting rate in the required pulse-height range was increased roughly in this ratio.

A further correction was required for the 60° π^- data. Owing to the thickness of the No. 4 light pipe, this particular channel was sensitive to Čerenkov radiation generated in the light pipe by electrons passing through it. The actual efficiency for electron detection was carefully measured, using the electrons accompanying the π^--meson beam as a source, for various angles of transmission of electrons through the light pipe, and the corresponding efficiency for detection of an electron pair was calculated. The resultant correction required for the cross section at this angle, for electron sensitivity of the light pipes of the detector telescope, was 0.026 ±0.020 mb sterad^{-1}. No such correction was necessary to the 45° π^- data.

Owing to minor changes in the equipment the mean scattering energy was not constant for all runs, varying from 39.1 to 41.8 Mev. This was allowed for by calculating the correction to be required, assuming our first approximate phase-shift solution to be correct, and then assuming the S-wave phase shifts were proportional to the momentum and the P-wave phase shifts were proportional to the cube of the momentum. The correction was found to be roughly 5% per Mev for π^+ scattering, but less than 1% per Mev for π^- scattering.

A further correction was necessary for the finite angular resolution of the apparatus. The angular resolution function was in general triangular in shape with a base width varying from 20° to 40°. Owing to the almost linear variation of the cross section with angle, the effect on the measured cross section was almost negligible for all angles except 163°. The correction for that angle was 1.5% and elsewhere was less than 0.005 mb sterad^{-1}. The values of the corrections for each angle and the base width of the angular resolution functions are given in Table I and of the cross sections in Table II.

V. CROSS-SECTION EXPRESSIONS

Van Hove[10] has analyzed pion-proton scattering and given expressions for differential cross sections in terms

ing large overcount, is very much less in the corresponding π^- run, and it is known that the cross section for production of two-pronged stars at this energy is much less for π^- that for π^+ mesons.

[10] L. Van Hove, Phys. Rev. 88, 1358 (1952).

TABLE II. Cross sections in mb sterad^{-1} and typical corrections in %.

	θ	Beam contamination	Counting losses	Absorp.	Gain of No. 4	Beam energy	Angular resolution function	Sensitivity to elec. pairs	$d\sigma/d\theta$ mb sterad^{-1}
π^+	53.0	3.5±1.5	0±1	3.9	−0.5±1	+0.7	+0.8		0.252±0.020
	69.1	2.5±1.5	0±1	2.3	0±1	+1.8	+0.3		0.354±0.025
	100.4	4.0±1.5	−2±3	2.73	1±2	+3.6	+0.5		0.777±0.038
	128.0	2±1	0±1	2.1	0±1	−1.8	−0.2		1.145±0.067
	141.7	2±1	0.5±1	1.8	−1±1	+0.3	−0.3		1.495±0.084
	163.5	5±1.5[a]	0.4±1[a]	0.2[a]		+0.3[a]	+1.34[a]		1.750±0.110
π^-	53.0	5±1.5	0±1	3.9	0±1	−0.4	−2.4	−9	0.338±0.047
	69.1	7±2	0±1	2.3	0±1	−0.3	−1.3	−12±6	0.281±0.038
	100.4	32±5	0±1	2.7	0±1	−3.3	−0.8	−4	0.148±0.028
	128.0	10±3	0±1	2.1	−1±1	+0.5	0.0	−8	0.112±0.042
	141.7	6.5±1.5	0.5±1	1.8	−1±1	+0.3	+0.1	−6	0.085±0.025

[a] Corrections given at 163.5° are for a typical run.

of a Born approximation point charge Coulomb amplitude, and an amplitude expressed in terms of phase shifts $\alpha_{ij}^{\pm}$ which we refer to here as composite phase shifts. He assumes a purely nuclear interaction for separation distances up to r_0 and neglects Coulomb forces over this range. These composite phase shifts then represent basically the nuclear interaction, but also the interference between nuclear and point Coulomb interaction, and the departure of the assumed electric potential from that of a point charge. They require than a small correction to make them purely nuclear. Van Hove gives the s-phase corrections while Salzman and Schnitzer[11] have calculated them for the p phases. The values in radians of these corrections $\Delta\alpha_{ij}$ at 41.5 Mev are given in Table III for two values of r_0.

Van Hove's nonrelativistic treatment of the scattering problem has been refined by Solmitz[12] through the introduction of relativistic considerations, and the modified Van Hove expressions for the differential cross sections assuming conservation of isotopic spin and limiting the analysis to s and p waves, are:

$$\frac{d\sigma}{d\Omega_{\pi^+\to\pi^+,\,\pi^-\to\pi^-}}=\left|\frac{1}{2ik}(P+Q\cos\theta)+f^{(nf)}(\theta)\right|^2+\left|\frac{1}{2ik}R\sin\theta+f^{(f)}(\theta)\right|^2,$$

where, for $\pi^+\to\pi^+$,

$$f^{(nf)}(\theta)=-\frac{e^2}{2p(V_\pi+V_p)\sin^2(\theta/2)}\left[1+\frac{1}{2}\frac{V_\pi V_p}{c^2}(1+\cos\theta)-\tfrac{1}{4}(2\mu_p-1)\frac{V_p^2}{c^2}(1-\cos\theta)\right],$$

$$f^{(f)}(\theta)=+\frac{e^2}{2p(V_\pi+V_p)\sin^2(\theta/2)}\times\left[\frac{\mu_p}{2}\frac{V_\pi V_p}{c^2}+\tfrac{1}{4}(2\mu_p-1)\frac{V_p^2}{c^2}\right]\sin\theta;$$

for $\pi^-\to\pi^-$, the signs of $f^{(nf)}(\theta)$ and $f^{(f)}(\theta)$ are reversed.

For $\pi^+\to\pi^+$:

$$P=\exp(2i\alpha_3^+)-1,$$
$$Q=\exp(2i\alpha_{31}^+)+2\exp(2i\alpha_{33}^+)-3,$$
$$R=\exp(2i\alpha_{33}^+)-\exp(2i\alpha_{31}^+);$$

for $\pi^-\to\pi^-$:

$$P=\tfrac{1}{3}[2\exp(i\alpha_1{}^N+i\alpha_1{}^-)+\exp(i\alpha_3{}^N+i\alpha_3{}^-)]-1,$$
$$Q=\tfrac{1}{3}[2\exp(i\alpha_{11}{}^N+i\alpha_{11}{}^-)+4\exp(i\alpha_{13}{}^N+i\alpha_{13}{}^-)+2\exp(i\alpha_{33}{}^N+i\alpha_{33}{}^-)+\exp(i\alpha_{31}{}^N+i\alpha_{31}{}^-)]-3,$$
$$R=\tfrac{1}{3}[2\exp(i\alpha_{13}{}^N+i\alpha_{13}{}^-)+\exp(i\alpha_{33}{}^N+i\alpha_{33}{}^-)-\exp(i\alpha_{31}{}^N+i\alpha_{31}{}^-)-2\exp(i\alpha_{11}{}^N+i\alpha_{11}{}^-)],$$

where μ_p=proton magnetic moment=2.793, V_π and V_p are the π and p velocities in the c.m. system, and $p=\hbar k=\pi$ momentum in the c.m. system. The above formulas for the $\pi^-\to\pi^-$ reaction have the following approximations[10]:

$$C^-=1;\quad (1-i\alpha)/(1+i\alpha)=1;\quad \exp(i\alpha_i{}^N-i\alpha_i{}^-)=1;\quad \exp(i\alpha_{ij}{}^N-i\alpha_{ij}{}^-)=1,$$

which means at 41.5 Mev an approximation of better than 1% for the cross sections. The formulas for the Coulomb correction to the phases are nonrelativistic and are calculated with the small phases approximation ($\cos\alpha\approx1$; $\sin\alpha\approx\alpha$):

$$\alpha^{\pm}=\alpha^N+\alpha^c,\quad \alpha^-=\alpha^N-\alpha^c.$$

For s waves:

$$\alpha_i{}^c=\alpha\,\ln 2\rho_0+\epsilon+2\alpha_i{}^N\,\mathrm{si}2\rho_0-\mathrm{Ci}2\rho_0,$$

for p waves:

$$\alpha_{ij}{}^c=\alpha\,\ln 2\rho_0-\frac{1}{2\rho_0}+\epsilon-1+2\alpha_{ij}{}^N\left(\mathrm{si}2\rho_0+\frac{1}{\rho_0}\cos 2\rho_0-\frac{1}{2\rho_0}\sin 2\rho_0\right)-\left(\mathrm{Ci}2\rho_0-\frac{1}{\rho_0}\sin 2\rho_0-\frac{1}{2\rho_0}\cos 2\rho_0\right),$$

[11] G. Salzman and H. Schnitzer (private communication).
[12] F. T. Solmitz, Phys. Rev. **94**, 1799 (1954).

where ϵ=Euler's constant=0.5772, and

$$\mathrm{Ci}x=-\int_x^\infty \frac{\cos x}{x}\alpha x$$

$$\mathrm{si}x=-\int_x^\infty \frac{\sin x}{x}\alpha x$$

$$\rho_0=kr_0=(p/m_\pi c)r_0(m_\pi c/\hbar)=R_0,$$

R_0 being the range of the nuclear interaction in units of $\hbar/m_\pi c$. $\alpha_i{}^N$ are the desired nuclear phase shifts. Figure 11 shows the Coulomb corrections to the α_3 and α_{33} phases as a function of r_0: they are rather large, especially for α_3, and they are strongly dependent on the assumed r_0 value. r_0 should actually be regarded as a parameter but this goes certainly beyond the precision of our data. In the absence of a definite value for r_0 we have chosen $r_0=\hbar/m_\pi c$ for our analysis, though there are some indications that it should be smaller. Test runs showed that the values of the scattering length $\alpha_3{}^N$ was decreased by 3.5% if r_0 was changed to $\frac{1}{2}\hbar/m_\pi c$ while the other lengths were altered by less than 1%.

VI. PHASE-SHIFT ANALYSIS

Suppose that we wish to determine k quantities, the unknown true values of which are $m_1 \cdots m_k$. We observe a certain number $n>k$ of linear functions f_i of these quantities, the true values of which are:

$$f_i{}^t=\sum_{j=1}^{k} a_{ij}m_j (i=1\cdots n),$$

where a_{ij} are certain known constants. Then it can be shown that the method of maximum likelihood determines a unique "best" solution for the unknown m_j $(j=1\cdots k)$, together with their complete error matrix, from the constants a_{ij}, the measured values X_i of the quantities f_i, and the errors on these measurements.

In our case we have one equation for each of n measured cross sections and 6 unknown phase shifts α_i (three if only π^+ data are used). Since the relationship between cross section and phases is not linear, a first-order Taylor expansion is made, namely

$$\sigma_i(\alpha_k{}^s+\delta\alpha_k)-\sigma_i(\alpha_k{}^s)=\sum_{j=1}^{6}\frac{\partial\sigma_i}{\partial\alpha_j}\delta\alpha_j \quad (i=1\cdots n).$$

This system is now in a form suitable for a least-squares treatment of the kind described above, but the

TABLE III. Corrections to phase shifts for two values of r_0.

r_0	$\Delta\alpha_1$	$\Delta\alpha_{11}$	$\Delta\alpha_{13}$	$\Delta\alpha_3$	$\Delta\alpha_{31}$	$\Delta\alpha_{33}$
$\hbar/m_\pi c$	0.0042	0.00026	0.0056	0.0054	0.00056	−0.0019
$\frac{1}{2}(\hbar/m_\pi c)$	−0.0009	0.00016	0.0005	0.0026	0.00045	−0.0029

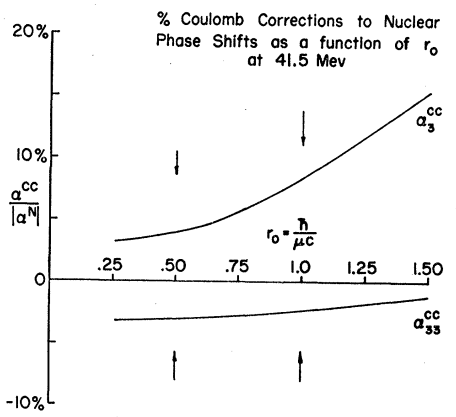

FIG. 11. Coulomb corrections.

coefficients $a_{ij}=\partial\sigma_i/\partial\alpha_j$ are only approximately constant. The experimental values,

$$X_i\equiv\sigma_i(\alpha_j{}^s+\delta\alpha_j)-\sigma_i(\alpha_j{}^s)=\sigma_i{}^m-\sigma_i{}^{\mathrm{calc}},$$

are now the differences between the measured cross sections $\sigma_i{}^m$ and the values $\sigma_i{}^{\mathrm{calc}}$ calculated from a starting set of phase shifts $\alpha_j{}^s$. The quantities m_j are the corrections $\delta\alpha_j$ to a starting set of phase shifts. Using this set of input data, the machine calculates the values $\sigma_i{}^{\mathrm{calc}}$ and $\partial\sigma_i/\partial\alpha_j$ and then derives a "best" set of corrections $\delta\alpha_j$. The goodness of fit is expressed by $\chi^2=\sum_{i=1}^{n} p_i\Delta_i{}^2$, where p_i is the weight for each measurement (taken as $p_i=\epsilon_i{}^{-2}$ with ϵ_i as the standard deviation of the measured cross section), and Δ_i is its deviation from the value calculated from the set of corrected phase shifts $\alpha_j{}^s+\delta\alpha_j$. The above procedure would give us the "best" solution $\alpha_j{}^s+\delta\alpha_j$ only if the values of $\partial\sigma_i/\partial\alpha_j$ were independent of α_j. As it is, it is necessary to repeat the analysis using $\alpha_j{}^s+\delta\alpha_j$ as the new $\alpha_j{}^s$.

The value of χ^2 from the second calculation is compared with that for the first and a further iteration carried out if they differ by more than 10^{-4}: otherwise the operations cease and the solution is printed out, together with various other quantities. Many intermediate steps are also printed out in order to have a continuous check on the analysis. Normally about four iterations are sufficient.

A solution may be visualized as a minimum on the χ^2 hypersurface. Each such minimum corresponds to a solution; the particular one found depends on the starting phases $\alpha_j{}^s$, since the machine moves to the closest relative minimum.

This method derives the standard errors from the slope of the hypersurface very near the minimum. The slightly different approach adopted by Anderson and Davidon[13] samples the hypersurface out to the value χ^2+1, and may, therefore, be affected by distortions in the surface which do not appreciably affect the slope near the minimum. Of course, what is of physical

[13] H. L. Anderson and W. C. Davidon, Nuovo cimento **5**, 1238 (1957).

TABLE IV. Results of phase-shift analysis for different combinations of data and for various values of ω_0^*. Column 1 gives the value of ω_0^*, column 2 gives the number of differential cross sections included in the analysis, column 3 gives letters which define the combinations of different energy data used for each analysis, while the last column shows the value of χ^2 found for that solution.

ω_0^*	No. of points	Comb.[a]	a_{31}^N	a_3^N	a_{33}^N	a_1^N	a_{11}^N	a_{13}^N	χ^2
2.17	11	A	-0.0477 ± 0.0068	-0.1005 ± 0.015	$+0.2337\pm0.0190$ f^2	$+0.1668\pm0.023$	$-0.016\ \pm0.11$	$-0.055\ \pm0.062$	3.39
2.17	29	B	-0.0439 ± 0.0053	-0.1100 ± 0.004	$+0.0879\pm0.0022$	$+0.1668\pm0.013$	-0.0381 ± 0.038	-0.0386 ± 0.0225	8.03
2.13	26	C	-0.0436 ± 0.0053	-0.1106 ± 0.004	$+0.0853\pm0.0022$	$+0.1716\pm0.022$	-0.0179 ± 0.11	-0.0486 ± 0.061	7.88
2.17	26	C	-0.0439 ± 0.0053	-0.1101 ± 0.004	$+0.0879\pm0.0022$	$+0.1713\pm0.022$	-0.0178 ± 0.11	-0.0492 ± 0.061	7.67
2.21	26	C	-0.0441 ± 0.0053	-0.1096 ± 0.004	$+0.0905\pm0.0023$	$+0.1711\pm0.022$	-0.0175 ± 0.11	-0.0496 ± 0.061	7.53
2.17	36	D	-0.0418 ± 0.0041	-0.1145 ± 0.0026	$+0.0877\pm0.0014$				21.25

[a] $A=6\ \pi^+$ and $5\ \pi^-$ at 41.5 Mev; $B=3\ \pi^+$ at 24.8 Mev; $3\ \pi^+$ at 31.5 Mev; $6\ \pi^+ + 5\ \pi^-$ at 41.5 Mev; $9\ \pi^+$ at 58 Mev and $3\ \pi^-$ at 65 Mev; $C=3\ \pi^+$ at 24.8 Mev; $3\ \pi^+$ at 31.5 Mev; $6\ \pi^+ + 5\ \pi^-$ at 41.5 Mev; $9\ \pi^+$ at 58 Mev; $D=3\ \pi^+$ at 24.8 Mev; $4\ \pi^+$ at 30 Mev; $3\ \pi^+$ at 31.5, Mev; $6\ \pi^+$ at 41.5 Mev $+6\ \pi^+$ at 58 Mev $+3\ \pi^+$ at 60.7 Mev $+11\ \pi^+$ at 150 Mev.

interest is the distorted shape of the contour χ^2+1, which bounds the allowable variation of the phase shifts. However, if an attempt is made to express this allowable range of variation in terms of standard errors, the distortion of the surface can result in absurdities in the analysis, such as negative variances. This may make it impossible to ascribe an error to the corresponding measurement. Also, of course, a distortion of the surface near the minimum may still allow an error to be calculated which is not a particularly accurate representation of the true errors of the phase shifts. Consequently, we feel that neither method of analysis has any overwhelming advantage over the other; the present one was chosen as being more suitable to the available computer.

Among the variety of information printed out by the computer were the components of the error matrix. These components are derived as follows from the coefficients $\partial\sigma_i/\partial\alpha_j$ of the final iteration, and the weights p_i. Defining

$$b_{rs}\equiv\sum_i p_i\frac{\partial\sigma_i}{\partial\alpha_r}\frac{\partial\sigma_i}{\partial\alpha_s},$$

$$C_{rs}\equiv\text{cofactor of } b_{rs} \text{ in the matrix } (b_{rs}),$$

$$B\equiv\text{determinant of matrix } (b_{rs}),$$

then the components of the error matrix are $E_{rs}=C_{rs}/B$ and consequently the standard error of α_j is $(C_{jj}/B)^{\frac{1}{2}}$.

It is perhaps worth pointing out that the treatment given in Cramer[14] assumes that only the relative standard errors of the measured values are known, and he uses the goodness of fit to determine the absolute values. In this work, we know the absolute standard errors, and hence the factor $(\chi^2/n-1)^{\frac{1}{2}}$ disappears from Cramer's equation for the standard error.

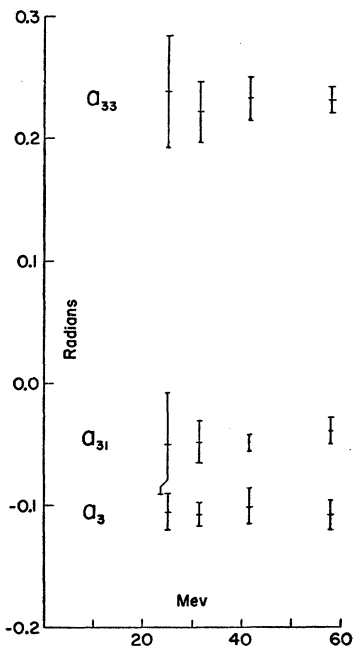

FIG. 12. $T=\frac{3}{2}$ scattering lengths as a function of energy.

VII. PHASE-SHIFT SOLUTIONS

(1) 41.5-Mev $\pi^\pm$ Data

Starting with values of α_3 and α_{33} which had been obtained through a preliminary study and which, happily, were in agreement with Orear's[15] recommendations, a least-squares analysis of the 41.5-Mev data was carried out, solving for the nuclear scattering lengths a_{ij}^N. The s phases were assumed to vary as η and the p waves as η^3. The results are given in line 1 of Table IV. The value of $\chi^2=3.4$ is reasonable compared with an expected value of 5.[16] The values of $D_+{}^b$ and $D_-{}^b$ calculated from these results are

$$D_+{}^b=0.104\pm0.033,\quad D_-{}^b=0.103\pm0.013.$$

[14] H. Cramer, *Elements of Probability Theory* (John Wiley and Sons, Inc., New York, 1955), pp. 235–240.

[15] J. Orear, Nuovo cimento 4, 856 (1956).

[16] Only Fermi-type solutions have been considered. In the analysis of the combined π^+ and π^- data, there is an ambiguity, equivalent to the Fermi-Yang ambiguity in the π^+ phase-shift analysis. For any solution $\alpha_{13}\alpha_{11}$ obtained from the relations, one has

$$2\alpha_{13}'+\alpha_{11}'=2\alpha_{13}+\alpha_{11},$$
$$2(\alpha_{13}'-\alpha_{11}')+(\alpha_{33}'-\alpha_{31}')=2(\alpha_{11}-\alpha_{13})+(\alpha_{31}-\alpha_{33}).$$

This alternative solution yields large values of α_{13}' and α_{11}' at 41.5 Mev (equivalent to $-\alpha_{13}\simeq\alpha_{11}\simeq0.120$) and we have therefore not listed these solutions.

(2) 24.8-, 31.5-, 41.5-, and 58-Mev π^+ Data

To test the assumed momentum dependencies, a solution was made of the 58-Mev π^+ differential cross sections of reference 5 and Sachs *et al.*[17] This yielded the values -0.038 ± 0.01, -0.107 ± 0.01, and 0.23 ± 0.01, respectively, for $a_{31}{}^N$, $a_3{}^N$ and $a_{33}{}^N$.

Miller and Ring[18] have obtained values of these scattering lengths from their measurements at 24.8 Mev as have Johnson and Camac[2] from their work at 31.5 Mev. All these values, together with ours of line 1 Table IV, are plotted against energy in Fig. 12. While the errors are large there is no obvious departure from constancy for any of the scattering lengths, which implies that the energy dependencies assumed, i.e., η for s and η^3 for p phases, are satisfactory for the data at hand.

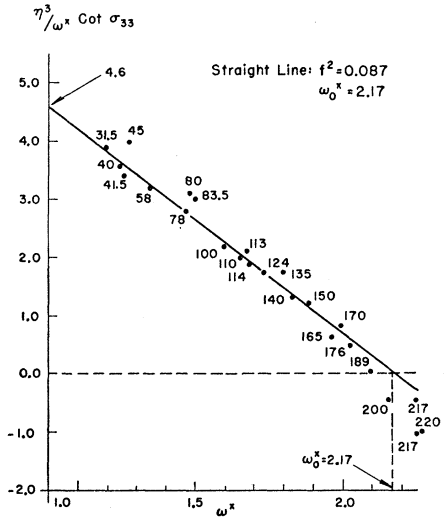

FIG. 13. Chew-Low plot [from W. B. Johnson and M. Camac, Atomic Energy Commission Report NYO-2169 (unpublished)]. References: 31.5 Mev—W. B. Johnson and M. Camac (to be published). 40 Mev—C. Angell and J. Perry, Phys. Rev. **91**, 1289 (1953). 41.5 Mev—This paper. 45 Mev—Orear, Lord, and Weaver, Phys. Rev. **93**, 575 (1954). 58 Mev—Bodansky, Sach, and Steinberger, Phys. Rev. **93**, 1367 (1954). 78 Mev—Anderson, Fermi, Martin, and Nagel, Phys. Rev. **91**, 155 (1953). 80, 83.5, and 100 Mev—G. Quareni *et al.*, *Proceedings of the CERN Symposium on High-Energy Accelerators and Pion Physics, Geneva, 1956* (European Organization of Nuclear Research, Geneva, 1956), Vol. II, pp. 230–232. 110 Mev—Anderson, Fermi, Martin, and Nagel, *op. cit.* 113 Mev—J. Orear, Phys. Rev. **96**, 1417 (1954). 114 and 124 Mev—G. Quareni *et al.*, *op. cit.* 135 Mev—H. L. Anderson *et al.*, *op. cit.* 140 Mev—J. J. Lord and A. B. Weaver, (private communication to H. L. Anderson). 150 Mev—Ashkin, Blaser, Feiner, and Stern, Phys. Rev. **101**, 1149 (1956). 165 Mev—H. L. Anderson and M. Glicksman, Phys. Rev. **100**, 268 (1955). 170 Mev—Ashkin, Blaser, Feiner, and Stern, *op. cit.* 176 Mev—Mukhin, Ozerov, Pontekorvo, Grigoriev, and Mitin, *Proceedings of the CERN Symposium on High-Energy Accelerators and Pion Physics, Geneva, 1956* (European Organization of Nuclear Research, Geneva, 1956), Vol. II, pp. 204–220. 189 Mev—Anderson, Davidson, Glicksman, and Kruse, Phys. Rev. **100**, 279 (1955). 200 Mev—A. I. Mukhin *et al.*, *op. cit.* 217 Mev—M. Glicksman, Phys. Rev. **94**, 1335 (1954). 217 Mev—H. Taft, Phys. Rev. **101**, 1116 (1956). 220 Mev—Ashkin, Blaser, Feiner, and Stern, Phys. Rev. **105**, 724 (1957).

[17] Sachs, Winick, and Wooten, Phys. Rev. **109**, 1733 (1958).
[18] D. Miller and J. Ring (private communication).

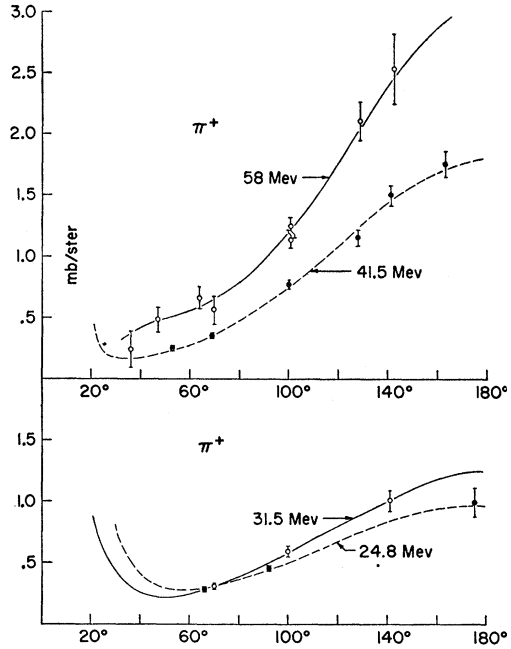

FIG. 14. π^+ experimental distributions with smooth curves calculated from Combination B coefficients.

(3) Combined Solutions

A solution was then made for 29 differential cross-section measurements: π^+ at 3 angles at 24.8 Mev of Miller and Ring,[3] π^+ at 3 angles at 31.5 Mev of Johnson and Camac,[2] π^+ at 9 angles at 58 Mev of Bodansky *et al.*[5] and Winick,[17] π^- at 3 angles at 65 Mev,[5] and our six π^+ and five π^- measurements at 41.5 Mev. Because of large errors the two smaller angle cross sections at 65 Mev were omitted. The η dependence was assumed for the s phases and η^3 for p phases except for α_{33} where a small-angle approximation of the Chew-Low dependency was used:

$$\alpha_{33}=\tfrac{4}{3}\eta^3 f^2\frac{1}{\omega^*(1-\omega^*/\omega_0{}^*)}.$$

This expression contains the two parameters $\omega_0{}^*$ and f^2, one of which must be given a value since our data are insufficient to fix both. Inspection of Fig. 13, a Chew-Low plot for the lower energies, suggests fixing $\omega_0{}^*$. We have done this, choosing 2.17 ± 0.00 for its value and solved for f^2. The results are given in the form of scattering coefficients in line 2 of Table IV and are labeled Combination B coefficients. To investigate their dependence on the value of $\omega_0{}^*$, solutions were obtained for each of the following values of $\omega_0{}^*$: 2.13, 2.17, and 2.21. The assemblage of differential cross sections actually used was slightly changed from that of the above Combination B by the omission of the three π^- 65-Mev points. The results given in the next three

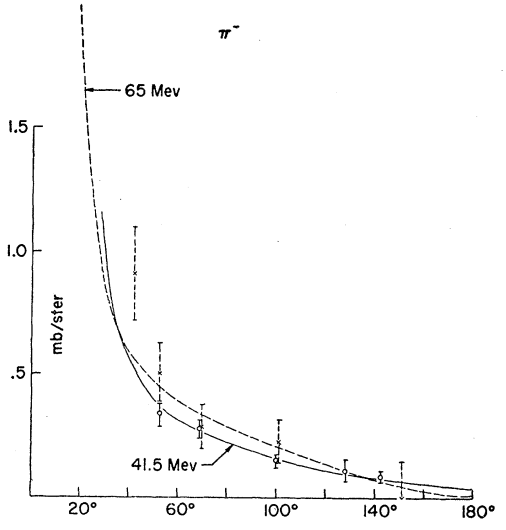

FIG. 15. π^- experimental distributions with smooth curves calculated from Combination B coefficients.

lines of Table IV show the phases to be quite insensitive to this variation in the value assumed for ω_0*. The values of χ^2 found in these runs are rather small. The most obvious explanation is that the errors on the published cross sections have been sometimes overestimated and include systematic errors.

Figure 14 shows the four experimental positive pion distributions that we have used and gives by means of the smooth curves the distributions calculated from the scattering coefficients of Combination B with the Coulomb contribution included. Figure 15 in similar manner shows the calculated π^- distributions for the two energies of 65 and 41.5 Mev where they can be compared with the measured cross sections previously mentioned.

VIII. TESTS OF THE $T=\frac{3}{2}$ PHASES

Measured π^+ differential distributions in the energy range from 25 to 58 Mev have been used to find values of these three phase shifts. Certain momentum dependencies have been assumed. A test of the latter is to use them to calculate scattering behavior at some reasonably distant energy.

We have calculated positive-pion total cross sections with their errors at various energies up to 150 Mev. In Fig. 16 these calculated values are indicated by the open error markers through which the smooth curve have been drawn. The measured point at 150 Mev of Ashkin[6] is given by the solid error marker, while the solid error markers at low energy are the values reported by Leonard and Stork.[7] The agreement is satisfactory, and the curve is indistinguishable from that given by Anderson.[19]

In Fig. 17 the π^+ differential distribution at 150 Mev of Ashkin[6] is displayed along with a curve which gives the distribution which we calculate. Again the agreement is satisfactory. Accordingly, we have combined the positive pion distributions of 24.8, 30,[20] 31.5, 41.5, 58, and 150 Mev and solved once again for the $T=\frac{3}{2}$ scattering coefficients. The exact Chew-Low dependence was used for α_{33} solving for f^2. The values are given in the lowest line of Table IV, and appear with smaller errors than those of line 1.

As an example, the error matrix E_{rs} as calculated by the computer for the Combination D solution is given in Table V.

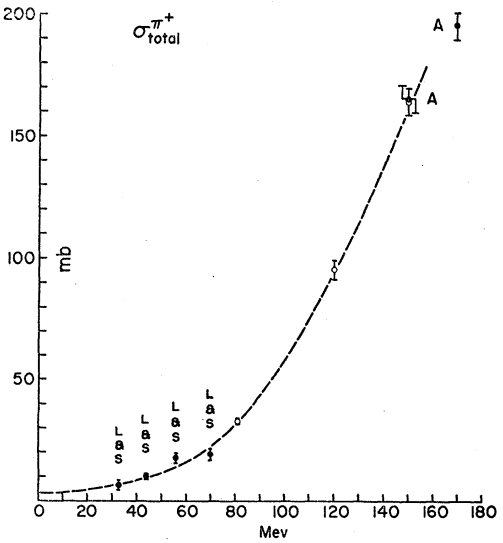

FIG. 16. π^+ total cross sections with smooth curves calculated from Combination B coefficients. The solid points with error markers are experimental points of Ashkin *et al.*[6] and Leonard and Stork.[7]

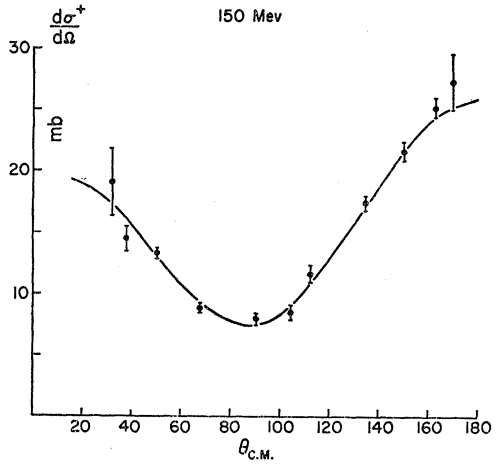

FIG. 17. 150-Mev π^+ differential cross section of Ashkin *et al.*[6] with smooth curve calculated from Combination B coefficients.

[19] H. L. Anderson, *Proceedings of the Sixth Annual Rochester Conference on High-Energy Nuclear Physics* (Interscience Publishers, New York, 1956).

[20] See reference 4; and Barnes, Winick, Miyake, and Kinsey, following paper [Phys. Rev. **117**, 238 (1960)].

For energies up to 150 Mev the present best values of these phases are then represented as follows:

$$\alpha_{31}{}^{N}=-(0.0418\pm0.0041)\eta^{3},$$

$$\alpha_{3}{}^{N}=-(0.1145\pm0.0026)\eta,$$

$$\tan\alpha_{33}{}^{N}=\tfrac{4}{3}\eta^{3}(0.0877\pm0.0014)\frac{1}{\omega^{*}(1-\omega^{*}/\omega_{0}{}^{*})}.$$

It should be emphasized that the above errors have meaning only to the extent that the several momentum dependencies are true. Values of $D_{+}{}^{b}$ calculated from these phases are given in Table VI. Since we will in Part II test the values of $D_{-}{}^{b}$ calculated from our phase shifts against the dispersion relation $D_{-}{}^{b}$ curve of Schnitzer and Salzman[21] we would like to compare the above values of $D_{+}{}^{b}$, with values the above authors would calculate from the corresponding $D_{+}{}^{b}$ dispersion relation. They do not give such a curve in their paper, but Schnitzer has most kindly provided us with a table of values from which this curve can be computed. We have used the same s-wave scattering lengths namely: $a_1=+0.205$ and $a_3=-0.114$ as we use in Part II and the same value of f^2, that is, 0.088. Thus the dispersion relation for $D_{+}{}^{b}$ is calculated from the same information as is the $D_{-}{}^{b}$ curve of Part II.

This $D_{+}{}^{b}$ dispersion relation is shown by the solid curve of Fig. 18 while the first four error markers show the points of Table V. The following three points are transcribed from the paper of Geffen.[22]

TABLE V. The error matrix E_{rs} for the Combination D phase-shift solution, in units of 10^{-6}.

	a_{31}	a_3	f^2
a_{31}	19.45	−3.08	−0.64
a_3	−3.08	6.67	2.43
f^2	−0.64	2.43	1.95

TABLE VI. $D_{+}{}^{b}$ with correlated errors calculated from the Combination D results of the last line of Table IV and the error matrix of Table V.

E_{Lab} (Mev)	$D_{+}{}^{b}$
30	0.0207±0.0044
50	0.1247±0.0062
100	0.4430±0.0098
150	0.4788±0.0086

[21] H. Schnitzer and G. Salzman, Phys. Rev. **112**, 1802 (1958).
[22] D. A. Geffen, Phys. Rev. **112**, 1370 (1958).

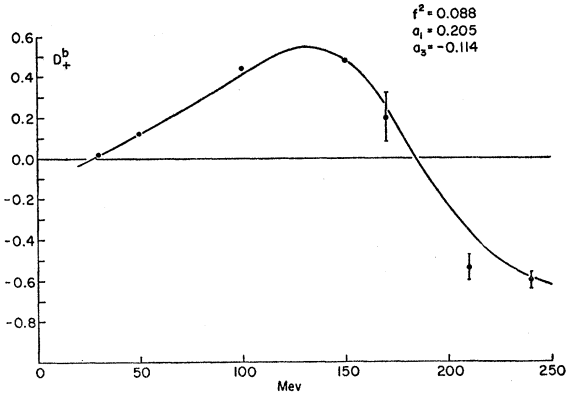

FIG. 18. $D_{+}{}^{b}$ *vs* pion energy. Smooth curves calculated after Schnitzer and Salzman.[21] The four lowest energy points are from Table V: the three high-energy ones are from Geffen.[22]

IX. CONCLUSION

Within the accuracy of the data, positive pion-proton scattering below resonance seems satisfactorily explained by the treatment together with the assumptions given above. In particular, simple momentum dependencies of the $T=\frac{3}{2}$ phase shifts, though not necessarily correct, are adequate. A test was made of the $T=\frac{1}{2}$ phase dependencies, by attempting to predict the 98-Mev differential cross sections, using the scattering lengths derived from the low-energy data. This prediction failed to fit the measured π^{-} differential cross sections at this energy.[23] It was clear then, that further investigation of the $T=\frac{1}{2}$ momentum dependencies was required.

X. ACKNOWLEDGMENTS

We are indebted to Pierre Noyes and George Salzman for many enlightening discussions, to Alex Wieber for his help in the design of and his careful work in the assembly of the various scattering setups, to Eric Chandler and Lionel Hodgson for their excellent work in constructing the more difficult of the crystals and light pipes, and to the operating crew under Fred Palmer for the many hours of cyclotron operation they furnished. One of us (G. G.) is indebted to the Fulbright Commission for a travel grant.

[23] Edwards, Frank, and Holt (to be published).